Hybrid orbital and numerical grid representation for electronic continuum processes: Double photoionization of atomic beryllium

F. L. Yip,[1] C. W. McCurdy,[1,2] and T. N. Rescigno[1]

[1]*Lawrence Berkeley National Laboratory, Chemical Sciences, and Ultrafast X-ray Science Laboratory, Berkeley, California 94720, USA*

[2]*Departments of Applied Science and Chemistry, University of California, Davis, California 95616, USA*

(Received 26 March 2010; published 13 May 2010)

A general approach for *ab initio* calculations of electronic continuum processes is described in which the many-electron wave function is expanded using a combination of orbitals at short range and the finite-element discrete-variable representation (FEM-DVR) at larger distances. The orbital portion of the basis allows efficient construction of many-electron configurations in which some of the electrons are bound, but because the orbitals are constructed from an underlying FEM-DVR grid, the calculation of two-electron integrals retains the efficiency of the primitive FEM-DVR approach. As an example, double photoionization of beryllium is treated in a calculation in which the $1s^2$ core is frozen. This approach extends the use of exterior complex scaling (ECS), successfully applied to helium and H_2, to calculations with two active electrons on more complicated targets. Integrated, energy-differential and triply-differential cross sections are exhibited, and the results agree well with other theoretical investigations.

DOI: 10.1103/PhysRevA.81.053407 PACS number(s): 32.80.Fb

I. INTRODUCTION

Numerical grid methods combining the finite-element discrete-variable representation (FEM-DVR) approach with exterior complex scaling (ECS) [1] have allowed effectively exact calculations of electron impact ionization [2] and double-photoionization cross sections for two-electron atomic [3] and molecular targets [4] over the last decade. The FEM-DVR approach has formed the basis of numerically accurate solutions of the time-dependent Schrödinger equation for such systems under the influence of ultrashort radiation pulses [5–7]. On the other hand, the success of atomic and molecular electronic structure calculations of many-electron systems depends on expressing those wave functions in terms of configurations with orthogonal orbitals. The configuration interaction (CI) method and its variants are orbital based, and that is the standard approach and the natural language of electronic structure theory.

Here, we describe a method that has the advantages of both approaches. It exploits the finite element aspect of the FEM-DVR to allow the construction of orbitals from only the DVR polynomial basis in the first few finite elements to describe electrons in bound orbitals. The remainder of DVR grid representation is left untouched and describes the continuum portions of the wave function. We have previously demonstrated that a particular advantage of the DVR approach is that the two-electron integrals in the DVR basis are given by simple formulas and are diagonal in the two pairs of indices that label them. That fact results in remarkable simplifications even when the DVR basis is transformed to atomic or molecular orbitals, as we will discuss below.

As a demonstration of this numerical method, we choose the relatively simple case of double photoionization (DPI) of the beryllium atom in which the orbital in the $1s^2$ core remains frozen. Since the $1s^2$ core electrons lie energetically far below the $2s$ valence shell and the mean value $\langle r \rangle$ of the $1s$ and $2s$ orbitals are very different [8], correlation effects between electrons occupying different shells are likely to be minimal. Thus, a reasonable approximation to double photoionization from beryllium allows for the valence electrons to be correlated separately from the closed-shell core electrons, and recent theoretical investigations on Be that have followed this approach to produce fully differential DPI cross sections include convergent-close coupling (CCC) [9], time-dependent close coupling (TDCC) [10], and the hyperspherical R-matrix method with semiclassical outgoing waves (HRM-SOW) [11]. Integral DPI cross sections have also been computed more recently using B-spline basis methods [12] as well as with the R-matrix-with-pseudostates (RMPS) method [13]. Each of these methods has been modified to account for the presence of core electrons in some way in order to apply these techniques to beryllium. Only limited experimental investigations of DPI from beryllium have been conducted [14–16].

In this work, we calculate cross sections for DPI from beryllium at 20 eV above the double-ionization threshold, and compare the resulting triply differential cross sections with those of other theoretical approaches using different core potential approximations and methods of solving DPI problem. In Sec. II, we describe the hybrid orbital and FEM-DVR basis numerical method and the resulting implementation of the ECS approach to solving the double-ionization problem. The method, used previously in ECS calculations on two-electron systems [2,3], of extracting the amplitudes pertaining to double ionization from the scattering wave function must be modified in the presence of the field of the frozen core, and these details are also given in Sec. II. Section III presents the calculated cross sections for DPI from beryllium, including the integral, energy-differential, and triply-differential cross sections. Finally, some brief conclusions and future work are discussed in Sec. IV.

II. THEORETICAL APPROACH

The amplitude for double photoionization is constructed from a solution of the driven equation for the first-order wave

function that is obtained when the radiation field is treated as a perturbation:

$$(E_0 + \omega - H)\Psi_{\rm sc}^{+} = (\boldsymbol{\epsilon} \cdot \boldsymbol{\mu})\Psi_0, \tag{1}$$

where H is the atomic Hamiltonian, ω is the photon frequency, $\boldsymbol{\epsilon}$ is the photon polarization vector, $\boldsymbol{\mu}$ is the electronic dipole operator, and Ψ_0 is the wave function describing the initial state of the atom with energy E_0. Equation (1) must be solved with outgoing-wave boundary conditions. Those boundary conditions are rigorously applied, as discussed for example in [2], by transforming the radial coordinates of the electrons according to the exterior complex scaling (ECS) transformation, which scales those coordinates by a phase factor beyond some radius R_0:

$$r \to \begin{cases} r, & r \leqslant R_0 \\ R_0 + (r - R_0)e^{i\theta}, & r > R_0. \end{cases} \tag{2}$$

This transformation causes wave functions with pure outgoing boundary conditions to decay exponentially beyond the exterior complex scaling radius R_0, thereby allowing the problem to be treated on a finite grid while preserving the true physical wave function inside of R_0.

For two-electron problems, we can solve Eq.(1) using an FEM-DVR description of the radial motion of the electrons [a radial DVR basis of functions $\chi_i(r)$] and a spherical harmonic basis $Y_{lm}(\Omega)$ to describe angular motion. The resulting description of electron-electron repulsion in this product basis is remarkably simple and efficient, because the radial two-electron integrals, as we shall see explicitly below, are diagonal in pairs of their four indices. That is the central reason why full CI in this large product basis is a practical computational approach to double-ionization problems.

To treat double-continuum processes in a many-electron atom, one would ideally like to expand the wave function in configurations in which two electrons are represented by the FEM-DVR product basis and the rest are represented by atomic orbitals. For a four-electron system, for example, we would have (suppressing the spin functions) an expansion of the form

$$\Psi = \sum_{\mathbf{n},i,j} C_{\mathbf{n},i,j} |\varphi_{n_1}(1)\varphi_{n_2}(2)\chi_i(r_3)Y_{l_i m_i}(\Omega_3)\chi_j(r_4)Y_{l_j m_j}(\Omega_4)|. \tag{3}$$

Immediately the question arises of how to construct a combined orbital and DVR basis such that all functions are mutually orthogonal, and how to perform the resulting two-electron integrals between the orbital and DVR basis functions. That question is present even if the same set of orbitals $\{\varphi_{n_i}\}$ appears in all the configurations, as would be the case in a frozen-core calculation. Without loss of generality, that is the case we treat here.

A. Hybrid orbital and FEM-DVR representation of the core and valence electrons

Treating an atomic problem with two active electrons and the rest occupying frozen orbitals requires a procedure to account for the interaction of the two valence electrons with the core. Two methods that have been previously utilized for double photoionization of beryllium include:

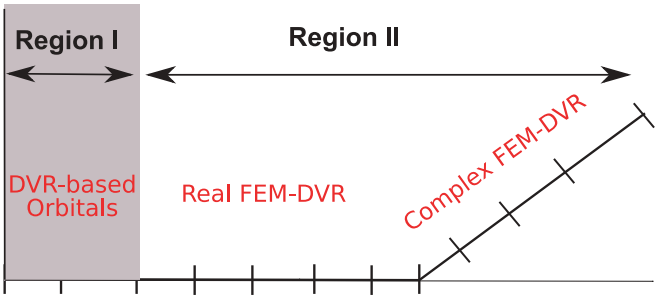

FIG. 1. (Color online) Sketch of hybrid basis constructed from DVR-based orbitals and the primitive finite-element discrete-variable representation.

(1) model potentials that represent the combined effects of core polarization and nuclear screening with a semiempirical local potential and (2) pseudopotentials which alter the one-electron residual ion (core + 1 electron) orbitals to force orthogonality back to the core orbitals. A more detailed description of the advantages and disadvantages of these two frameworks can be found in Ref. [11]. Briefly, the limitations on model potentials are the need to remove contributions to the wave function from unphysical states (see below), while the limitation of pseudopotentials is the arbitrary but incorrect behavior of the nodeless valence orbital in the core region resulting in inaccurate cross sections calculated in gauges that emphasize the region near the nucleus.

The present treatment uses neither model nor pseudopotentials, but rather constrains the core electrons to doubly occupy a set of orbitals $\{\varphi_o\}$ and then properly accounts for direct and exchange interactions with the valence electrons. The doubly occupied orbitals are obtained from a Hartree-Fock calculation on the neutral target atom and then reexpanded in an FEM-DVR basis using only the DVR functions in the first two or three finite elements. The idea is sketched in Fig. 1.

In the case of beryllium, there is only one such orbital, and we note in passing that the it is quite insensitive to whether it is derived from a Hartree-Fock treatment of Be^{++}, Be^{+}, or neutral Be, indicating that the properties of the $1s^2$ closed shell are dominated by the nuclear attraction and insignificantly polarized by the $2s$ orbital penetration into the core region.

With the orbital restriction on the core electrons, the effective Hamiltonian for the two active electrons can be written (atomic units throughout unless otherwise indicated):

$$H = h(1) + h(2) + \frac{1}{r_{12}}, \tag{4}$$

where $1/r_{12}$ is the Coulomb repulsion between the active electrons. The one-body operator h is

$$h = T - \frac{Z}{r} + \sum_{\rm o} 2J_{\rm o} - K_{\rm o}, \tag{5}$$

where T is the one-electron kinetic energy operator, Z/r the nuclear attraction (with $Z = 4$ in the present case) and $2J_{\rm o}$ and $K_{\rm o}$ are the direct and exchange components of the core interaction with the valence electrons, respectively. Explicitly, the Coulomb operator for orbital $\varphi_{\rm o}$ is given by

$$J_{\rm o}(\mathbf{r}) = \int \frac{|\varphi_{\rm o}(\mathbf{r}')|^2}{|\mathbf{r} - \mathbf{r}'|} d\mathbf{r}', \tag{6}$$

while the nonlocal exchange operator acting on an orbital $\chi(\mathbf{r})$ is

$$K_o(\mathbf{r})\chi(\mathbf{r}) = \varphi_o(\mathbf{r}) \int \frac{\varphi_o^*(\mathbf{r}')\chi(\mathbf{r}')}{|\mathbf{r}-\mathbf{r}'|} d\mathbf{r}'. \quad (7)$$

In our previous studies of DPI in helium [17] and H^- [3], the two-electron Hamiltonian was diagonalized in a product basis of primitive FEM-DVR radial functions times spherical harmonics for each electron, which gives a full configuration-interaction (CI) treatment of the problem in the underlying basis. In the present case, however, using an unconstrained primitive basis with the effective two-electron Hamiltonian in Eq. (5) would lead to the appearance of unphysical (bosonic) states that result from overpopulation of the doubly occupied orbitals by more than two electrons, and so the formulation must be modified to impose strict orthogonality between the core and valence electrons.

An obvious way to accomplish this would be to carry out the calculation in an atomic orbital (AO) basis, where the AOs are expressed as linear combinations of DVR functions, and simply exclude the doubly occupied core orbitals from all configurations. Such an approach, however, fails to take advantage of a key simplification in the calculation of two-electron integrals when using FEM-DVR basis functions; namely, as mentioned above, that the radial portion of the electron-electron repulsion matrix elements are diagonal in the DVR index of each electron [2]. Specifically,

$$\langle ij|V_\lambda|kl\rangle \equiv \int dr dr' \chi_i(r_1)\chi_j(r_1)\frac{r_<^\lambda}{r_>^{\lambda+1}}\chi_k(r_2)\chi_l(r_2) = \delta_{ij}\delta_{kl} f(i,l), \quad (8)$$

when $\chi(r)$ is a DVR function and $f(i,l)$ is given in [2]. In the present context of a calculation on Be, we can use primitive DVRs for all basis functions with $\ell \neq 0$, since there are no restrictions in those symmetries. In general for closed shell cores, we can use primitive DVRs for all the angular momenta not appearing in doubly occupied core orbitals. In the case of Be, for the $\ell = 0$ functions, we first make use of the fact that the $1s$ orbital is nonzero only over a limited range near the nucleus, so we can choose a finite element boundary beyond which ϕ_{1s} is effectively zero and form a set of orthonormal s-type AOs ϕ_α using only primitive DVR functions ($\chi_i, i = 1, \ldots, M$) that lie within the relevant range,

$$\varphi_\alpha(r) = \sum_{j=1}^{M} U_{\alpha j}\chi_j(r). \quad (9)$$

as indicated in Fig. 1. Because the DVR functions are orthogonal, the orbitals created out of the first M DVR functions by this unitary transformation are not only orthogonal to each other; they are orthogonal to all the remaining primitive FEM-DVR functions in the basis.

$$\langle \varphi_\alpha|\chi_k\rangle = 0 \quad k > M. \quad (10)$$

If we consider, for example, two-electron matrix elements where all four basis functions have $\ell = 0$, then they can be grouped into six classes:

(1) $\langle \chi_i\chi_j||\chi_k\chi_l\rangle$ – all primitive DVR,
(2) $\langle \varphi_\alpha\varphi_\beta||\varphi_\gamma\varphi_\delta\rangle$ – four orbitals,
(3) $\langle \chi_i\chi_j||\phi_\alpha\varphi_\beta\rangle$ – two orbitals,
(4) $\langle \chi_i\chi_j||\chi_k\varphi_\alpha\rangle$ – one orbital,
(5) $\langle \varphi_\alpha\chi_i||\varphi_\beta\varphi_\gamma\rangle$ – three orbitals,
(6) $\langle \varphi_\alpha\chi_i||\varphi_\beta\chi_j\rangle$ – two orbitals.

Classes (4)–(6) are zero because they pair an atomic orbital with index less than or equal to M with a primitive DVR which, by construction, has index greater than M. The class-(1) matrix elements are those given by Eq. (8). The class-(2) integrals are written, using Eqs. (8) and (9), as

$$\langle \varphi_\alpha\varphi_\beta||\varphi_\gamma\varphi_\delta\rangle = \sum_{i,j=1}^{M} U_{\alpha i}U_{\beta i} f(i,j) U_{\gamma j}U_{\delta j}. \quad (11)$$

Because the primitive integrals are diagonal in the DVR indices for each electron, there are only two sums needed to evaluate the class-(2) matrix elements directly. The class-(3) matrix elements involve only a single sum in their evaluation. Matrix elements involving both s-type and higher ℓ-type orbitals can be similarly calculated and never involve sums over more than two indices. The "four-index transformation," familiar from electronic structure theory, is reduced in this approach to an effective two-index transformation.

These simplifications are a result of the compact support of the primitive DVR polynomial basis functions $\chi_i(r)$ within the finite-element boundaries and will lead to an efficient CI representation of many electron systems in which two electrons can be in the continuum.

B. Calculation of the double-photoionization amplitudes

The scattered wave (as well as the initial target state) is expanded in a product basis formed from FEM-DVR functions and spherical harmonics:

$$\Psi_{sc}^+ = \sum_{l_1m_1}\sum_{l_2m_2} \frac{\psi_{l_1m_1,l_2m_2}(r_1,r_2)}{r_1r_2} Y_{l_1m_1}(\hat{\mathbf{r}}_1)Y_{l_2m_2}(\hat{\mathbf{r}}_2). \quad (12)$$

In the case of beryllium, having projected the $1s$ orbital (but not the other φ_α orbitals) from the basis, we diagonalize the effective two-electron Hamiltonian in ^{1}S symmetry to obtain the Be ground state and then construct the Hamiltonian in ^{1}P symmetry to solve Eq. (1). The scattered wave Ψ_{sc}^+ is then used to compute the amplitudes for double photoionization. As described earlier [2,4,17], this can be accomplished by using a testing function that not only extracts the double-ionization amplitude, but also removes any spurious contributions from single ionization at the same photon energy that could contaminate the desired result. For helium, the appropriate testing functions are simply the continuum Coulomb wave functions $\Phi_{(c)}^+(\mathbf{k},\mathbf{r})$ with $Z = 2$, while for H_2 the testing functions are continuum states of H_2^+.

Following a similar logic, the testing functions that will separate the double-ionization continuum from the other energetically open channels must be continuum states of Be^+, which are orthogonal to the bound states of the singly charged ion produced by single ionization. To construct these states, we follow a procedure similar to the one used to treat DPI of

H_2 [4]. The full testing function $\Phi^+(\mathbf{k},\mathbf{r})$ is decomposed as the sum

$$\Phi^+(\mathbf{k},\mathbf{r}) = \chi(\mathbf{k},\mathbf{r}) + \Phi^+_{(c)}(\mathbf{k},\mathbf{r}) \tag{13}$$

of a scattered part $\chi(\mathbf{k},\mathbf{r})$ and a long-range Coulomb wave function $\Phi^+_{(c)}(\mathbf{k},\mathbf{r})$ with asymptotic charge $Z=2$ because the long-range behavior of the direct operator for the occupied $1s^2$ core is to screen the the $Z=4$ nucleus of beryllium,

$$2J_{1s}(r) \underset{r_i\to\infty}{\sim} \frac{2}{r}. \tag{14}$$

Because the exchange operator K_{1s} in Eq. (5) has the range of the $1s$ orbital, there is no complication in solving a driven Schrödinger equation of the form

$$\left(\frac{k^2}{2} - h\right)\chi(\mathbf{k},\mathbf{r}) = \left(h - \frac{k^2}{2}\right)\Phi^+_{(c)}(\mathbf{k},\mathbf{r}) = \left(-\frac{2}{r} + 2J_{1s} - K_{1s}\right)\Phi^+_{(c)}(\mathbf{k},\mathbf{r}), \tag{15}$$

where $k^2/2$ is the energy of the electron. To be able to describe the amplitude for an arbitrary direction of the momentum, we expand the testing function as well as the Coulomb function in partial waves:

$$\Phi^+(\mathbf{k},\mathbf{r}) = \sum_{\ell,m} \frac{\varphi^k_\ell(r)}{r} Y^*_{\ell m}(\hat{\mathbf{k}}) Y_{\ell' m}(\hat{\mathbf{r}}), \tag{16}$$

$$\Phi^+_{(c)}(\mathbf{k},\mathbf{r}) = \left(\frac{2}{\pi}\right)^{1/2} \sum_{\ell,m} \frac{i^\ell e^{i\eta_\ell}}{kr} \phi^{(c)}_{\ell,k}(r) Y_{\ell m}(\hat{\mathbf{r}}) Y^*_{\ell m}(\hat{\mathbf{k}}), \tag{17}$$

where $\phi^{(c)}_{\ell,k}(r)$ is a radial Coulomb function behaving asymptotically as

$$\phi^{(c)}_{\ell,k}(r) \to \sin[kr + (Z/k)\ln(2kr) - \ell\pi/2 + \eta_\ell(k)], \tag{18}$$

for $r\to\infty$ with Coulomb phase η_ℓ given by

$$\eta_\ell(k) = \arg\Gamma(\ell + 1 - iZ/k), \tag{19}$$

with $Z=2$. This decomposition leads to a radial driven Schrödinger equation for each partial-wave component of the testing function:

$$\left(\frac{k^2}{2} - h_\ell\right)\varphi^k_\ell(r) = \left(-\frac{2}{r} + 2J_{1s} - K_{1s}\right)\frac{\phi^{(c)}_{\ell,k}(r)}{kr}. \tag{20}$$

The double-photoionization amplitude to produce outgoing electrons with momenta $\mathbf{k}_1$ and $\mathbf{k}_2$ is expressed as the coherent sum of partial-wave amplitudes [3,17]:

$$f(\mathbf{k}_1,\mathbf{k}_2) = \sum_{l_1,m_1}\sum_{l_2,m_2}\left(\frac{2}{\pi}\right) i^{-(l_1+l_2)} e^{i\eta_{l_1}(k_1)+i\eta_{l_2}(k_2)} \tag{21}$$

$$\times \mathcal{F}_{l_1,l_2,m_1,m_2}(k_1,k_2) Y_{l_1 m_1}(\hat{\mathbf{k}}_1) Y_{l_2 m_2}(\hat{\mathbf{k}}_2), \tag{22}$$

where the radial amplitudes $\mathcal{F}_{l_1,l_2,m_1,m_2}(k_1,k_2)$ are evaluated along a hypersphere ρ_0 in the (r_1,r_2) plane just inside the ECS turning point R_0. The radial amplitudes are computed using a surface-integral formulation that amounts to the integration of the Wronskian between the scattered wave decomposition of the full solution $\psi_{l_1 m_1, l_2 m_2}(r_1,r_2)$ and the partial-wave testing functions [2,3,17]:

$$F_{l_1,l_2,m_1,m_2}(k_1,k_2) = \frac{\rho_0}{2}\int_0^{\pi/2}\left[\varphi^{k_1}_{l_1}(r_1)\varphi^{k_2}_{l_2}(r_2)\frac{\partial}{\partial\rho}\psi_{l_1 m_1, l_2 m_2}(r_1,r_2)\right. \tag{23}$$

$$\left. - \psi_{l_1 m_1, l_2 m_2}(r_1,r_2)\frac{\partial}{\partial\rho}\varphi^{k_1}_{l_1}(r_1)\varphi^{k_2}_{l_2}(r_2)\right]\Big|_{\rho=\rho_0} d\alpha. \tag{24}$$

C. Definition of the cross sections from the radial amplitudes

The triply-differential cross section (TDCS) for double photoionization is computed from the amplitudes in Eq. (21) by

$$\frac{d^3\sigma}{dE_1 d\Omega_1 d\Omega_2} = \frac{4\pi^2\omega}{c} k_1 k_2 |f(\mathbf{k}_1,\mathbf{k}_2)|^2, \tag{25}$$

in the length gauge. Integration of the TDCS over the angles Ω_1 and Ω_2 of the electrons yields the singly differential cross section (SDCS) which describes the cross section as a function of the energy sharing $E_1 + E_2 = E$ alone. This is given simply by

$$\frac{d\sigma}{dE_1} = \frac{4\pi^2\omega}{c} k_1 k_2 \left(\frac{2}{\pi}\right)^2 \sum_{l_1 m_1}\sum_{l_2 m_2} |\mathcal{F}_{l_1,l_2,m_1,m_2}(k_1,k_2)|^2. \tag{26}$$

With this definition of the SDCS, the total integrated cross section for double photoionization at photon energy ω with excess energy $E = \omega + E_0$ is

$$\sigma = \int_0^E \frac{d\sigma}{dE_1} dE_1. \tag{27}$$

Since the SDCS is symmetric about $E/2$, previous experimental and theoretical treatments have often scaled the SDCS according to

$$\frac{d\tilde{\sigma}}{dE_1} = 2\frac{d\sigma}{dE_1}, \tag{28}$$

so that the total DPI cross section is computed by integrating the scaled cross section over half the available energy range:

$$\sigma = \int_0^{E/2} \frac{d\tilde{\sigma}}{dE_1} dE_1. \tag{29}$$

To compare with the previous theoretical calculations on beryllium, we continue to use the latter definition of the SDCS here.

III. DOUBLE PHOTOIONIZATION OF BERYLLIUM

A. Computational details

The driven Schrödinger equation in Eq. (1) was solved with a radial grid using 15th order DVR with real FEM boundaries at 2.0, 7.0, 12.0, 20.0, 30.0, and 40.0 bohr, followed by two complex finite elements with the end of the grid located at $r = 70.0$ bohr. The ECS rotation angle in Eq. (2) was 30.0°. The atomic s-type orbitals used in the construction and projection of the $1s$ orbital, as outlined in Sec. II A, were built using DVR points only from the first two elements (i.e., up to $r = 7.0$ bohr). To construct the Be ground state, we used all

radial grid points out to $r = 20.0$ bohr, along with an angular basis consisting of all lm pairs for both electrons consistent with the ^1S symmetry of the initial state up through $l_{max} = 7$. With these parameters, the double-ionization potential of ground-state beryllium is calculated here to be 1.007 90 atomic units (a.u.), compared to the calculated value of 1.011 80 a.u. [18,19]. For the final state ^1P continuum, we of course use the full ECS grid. To connect the final state with the bound state via the dipole operator, $l_{max} = 8$ was chosen for the final ^1P continuum.

B. Convergence tests

Convergence data for various parameters of the beryllium DPI calculation is presented in Fig. 2. The TDCS plotted in these figures shows the cross section for a particular energy sharing with one electron fixed as the other is varied in the plane defined by the fixed electron and the polarization vector. In Fig. 2, the fixed electron energy and direction are $E_1 = 30$ eV and $\theta_1 = 20^\circ$, respectively. All angles are measured relative to the linear polarization direction of the photon.

The upper-left panel of Fig. 2 shows convergence with respect to the angular basis. The cross sections appear to be converged with $l_{max} = 7$, being graphically indistinguishable from the $l_{max} = 8$ results. The upper-right panel shows the gauge dependence of the calculated cross sections. We note that the height of the dominant peak varies by a few percent between the length and velocity gauges. This differs from our earlier calculations on helium, which gave identical results in length, velocity, and acceleration gauges [17]. The small differences seen here are due to the emphasis that a particular gauge selection places on the inner region of the wave function, and the fact the core electrons are restricted

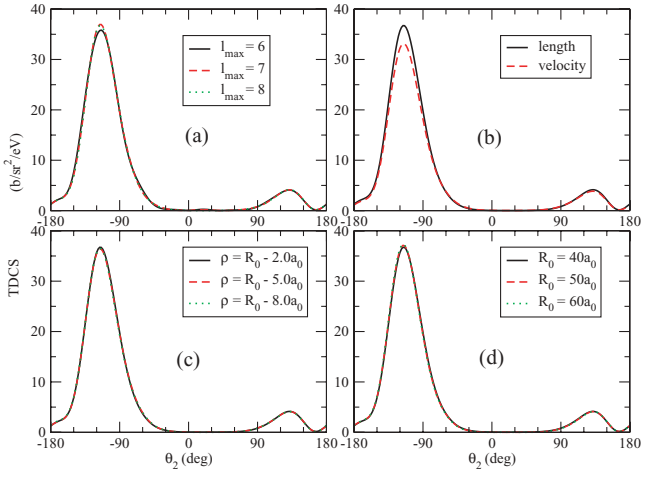

FIG. 2. (Color online) Convergence tests for DPI of beryllium. The TDCS above were calculated with one outgoing electron fixed with 65% energy sharing of 20-eV available excess energy at the angle $\theta_1 = 20^\circ$. Clockwise from upper-left panel shows (a) convergence with respect to the angular expansion basis l_{max}, (b) gauge representation of the dipole operator, (d) size of the purely real ECS radial grid R_0, and (c) extraction radius ρ for evaluation of the DPI partial-wave amplitudes. Cross sections are in units of barns (b) per eV per steradian (sr); 1 b = 10^{-24} cm^2. R_0 and ρ are in units of a_0; 1 $a_0 = 0.529 \times 10^{-8}$ cm.

to doubly occupy the same orbital. Calculations performed with model potentials [9–11], which do not represent the short-range dynamics near the nucleus with any fidelity, show a much larger gauge dependence in the calculated cross sections. Evidently, our particular representation of the core-valence interaction impacts the results only slightly. For consistency with comparisons to other theoretical calculations of DPI from beryllium, all results subsequently presented are shown in the length gauge.

The lower-left panel of Fig. 2 shows that the calculated TDCS does not depend on the location of the arc ρ along which the partial wave amplitudes in Eq. (22) are extracted. The lower-right panel also shows that the cross sections computed do not vary as the size of the radial grid is increased by extending the ECS turning point R_0. Taken together, these panels indicate that a suitable radial and angular basis has been selected and produces results that do not change, thus signaling convergence of the results with respect to the parameters of the calculation.

C. Total cross section

Most of the data in the literature for DPI of beryllium concerns the integral cross section. Figure 3 presents much of the existing theoretical and experimental data. Present results (stars) are shown along with fitted RMPS results [13] (solid curve), CCC results [9] (solid circles), TDCC results [10] (solid squares), B-spline results [12] (solid triangles), and experimental results [16] (solid diamonds). For clarity, results calculated by the HRM-SOW method [11] in various gauges are not shown, but generally agree with these results, differing only by slightly larger magnitudes closer to threshold as has been observed before [20]. Overall agreement between the different theoretical treatments and between theory and the few experimental values is good. The data indicates that the maximum in the cross section occurs in the range of ~12 eV above the DPI threshold. The results calculated in the present work agree very well with the calculation of Laulan and Bachau [12] over the energy range above the maximum in the cross section, differing most on the rising shoulder of the cross section near 5 eV.

D. SDCS results at 20-eV above threshold

The single differential cross section (SDCS) for DPI of beryllium at 20-eV above threshold is shown in Fig. 4 . Also displayed are SDCS calculations from TDCC [10] and HRM-SOW [11] treatments, both calculated in the length gauge. The present results are in better agreement with the TDCC results, differing only in the depth of the "smile" in the cross section at equal energy sharing. In contrast to the present results and to the TDCC results, the HRM-SOW calculation gives an SDCS that is relatively flat.

E. TDCS results at 20-eV above threshold

For the triply differential cross sections that are presented in the following section, we compare our length gauge results directly with TDCC results calculated in the same gauge [10]. We note that length-gauge results from the HRM-SOW study

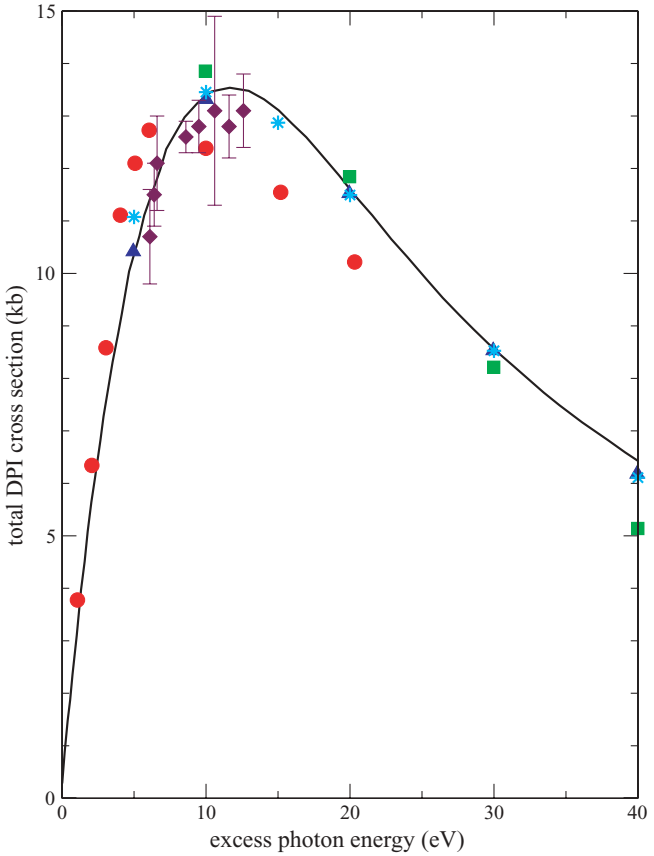

FIG. 3. (Color online) Total DPI cross section from beryllium at various energies. Stars give the present results, the solid curve is a polynomial fit to RMPS calculation [13] of Griffin *et al.*, solid circles are the CCC results of Kheifets and Bray [9], solid squares are the TDCC results of Colgan and Pindzola [10], solid triangles are the *B*-spline results of Laulan and Bachau [12], and solid diamonds with error bars are the experimental measurements of Wehlitz *et al.* [16]. 1 kb $= 10^{-21}$ cm^2.

[11], while close in shape to the present results, are generally 10%–20% higher at the major peaks.

Figure 5 shows TDCS at 20-eV excess photon energy for equal energy sharing between the ejected electrons. This case represents the highest degree of electron correlation in the final state. Each of the panels displays the TDCS for a fixed direction of one of the electrons $\theta_1 = 0°$, 30°, 60°, and 90°, with all angles measured relative to the linear polarization direction and in the same plane. The angular distributions that result for DPI of beryllium bear a remarkable similarity to those observed for helium, both showing a similar pattern in the location and relative heights of the major and minor peaks, indicating that the gross features of the angular patters arise mostly as a consequence of the atomic state symmetry [21]. The relative widths of the TDCS peaks in He and Be, however, show considerable differences, the latter being considerably narrower. It has been argued [9,11] that these differences can be related to the stronger effect of initial state electronic correlations in the case of beryllium, as reflected in the behavior of the parametrized gerade component of the DPI amplitudes for the two systems [22]. An alternative explanation has also been given [23], which states in essence that the strength

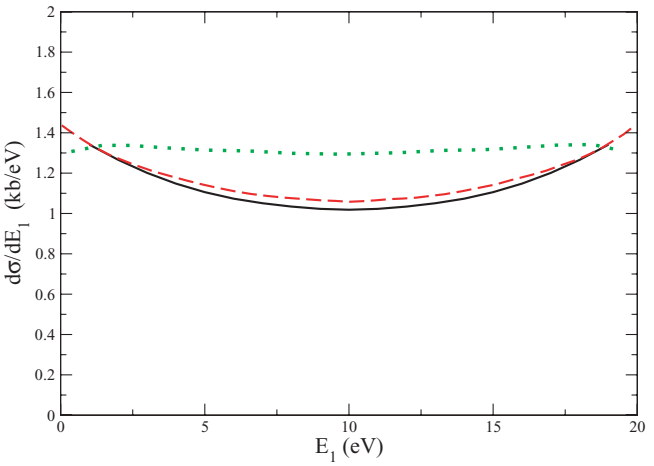

FIG. 4. (Color online) Single differential cross section (SDCS) results for DPI of beryllium at 20 eV excess photon energy. The solid curve gives the present results, the dashed curve shows the results of Colgan and Pindzola [10], the dotted curve shows the HRM-SOW results of Citrini *et al.* [11].

of the angular correlation in DPI comes primarily from the momentum distribution of the corresponding orbital of the singly ionized target, which is considerably narrower for the 2*s* orbital in Be^+ than for the 1*s* orbital in He^+.

The present results are seen to agree very well with the TDCC results, both in magnitude and in the angular distribution profile. Furthermore, both theoretical results exhibit the signature of a parity selection rule whose consequence at equal energy sharing prohibits the electrons from being ejected back-to-back [24], as can be seen in each of the four panels of Fig. 5. It is noteworthy that the length gauge results from both studies agree almost exactly despite different representations of the valence-core interaction, indicating

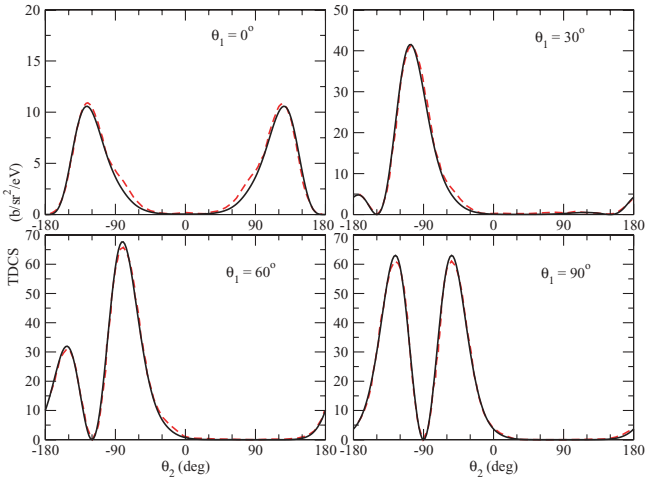

FIG. 5. (Color online) Triply differential cross section (TDCS) results for DPI of beryllium at 20-eV excess photon energy. The electrons share equal amounts of energy $E_1 = E_2 = 10$ eV. Each of the panels shows a different fixed value of the direction of the first electron θ_1. The solid curve shows the present results and the dashed curve shows the results of Colgan and Pindzola [10].

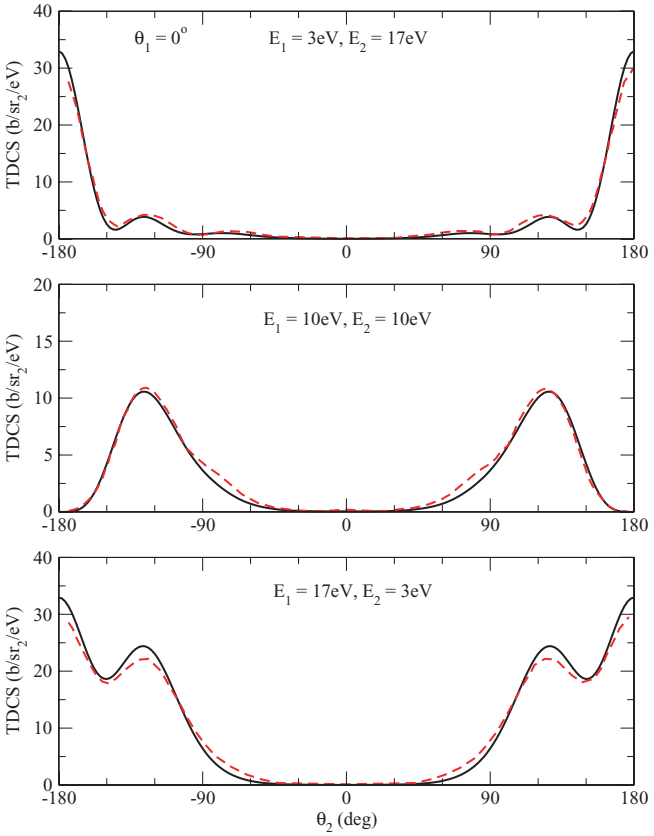

FIG. 6. (Color online) Triply differential cross section (TDCS) results for DPI of beryllium at 20-eV excess photon energy. The angle of the first electron is fixed along the polarization direction $\theta_1 = 0^\circ$. Each panel displays results as the energy sharing is varied: from top to bottom, the fixed electron carries 15%, 50%, and 85% of the available energy, respectively. The solid curve shows the present results and the dashed curve gives the results of Colgan and Pindzola [10].

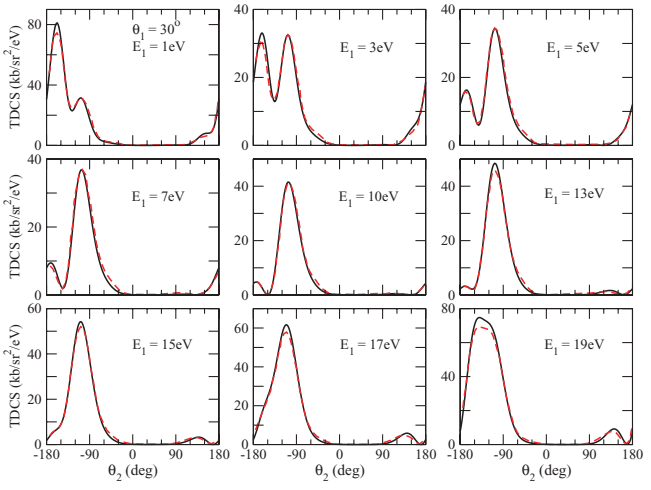

FIG. 7. (Color online) Triply differential cross section (TDCS) results for DPI of beryllium at 20-eV excess photon energy. The angle of the first electron is fixed at $\theta_1 = 30^\circ$. Each panel displays results as the energy sharing allocated to the first electron is varied from $E_1 = 5\%$ in the upper-left panel through $E_1 = 95\%$ in the lower-right panel. The solid curve shows the present results, whereas the dashed curve gives the results of Colgan and Pindzola [10].

that at this excess photon energy the dynamics of double photoionization are mostly dominated by the accuracy of the $2s$ orbital in the valence region and not over the range of the $1s$ orbital.

Figure 6 shows TDCS results at 15%, 50%, and 85% energy sharing, with the fixed electron aligned with the photon polarization direction. There is again excellent agreement with the TDCC results. Furthermore, the cross sections again bear a striking similarity to DPI from helium considered under similar conditions.

The final set of results displayed in Fig. 7 shows the TDCS for nine energy sharings when the angle of one electron is fixed at $\theta_1 = 30^\circ$. Once again, the angular distributions and relative peak heights of the cross sections are very similar to those for helium DPI. Agreement with the TDCC results is again very good, with only small differences visible in the maximum peak heights at the energy-sharing extremes. The best agreement occurs at equal energy sharing, similar to the results in Fig. 6.

IV. CONCLUSIONS

The triply differential, singly differential, and integral cross sections for double photoionization from beryllium presented here agree very well with those previously published [9–13]. The results indicate that beryllium DPI produces angular distributions and relative cross section magnitudes that are quite similar to those for helium DPI at the same excess photon energy.

Comparison with the results of other theoretical studies that employed model potentials to replace the core electrons shows that the calculated cross sections are similar, provided the length gauge is used in the comparison. This further supports the notion that the core and valence electrons are truly distinct with correlation between the inner and outer shells being negligible. Thus, DPI from the valence shell proceeds much like in helium.

While the differential DPI cross sections from the ground-states of He and Be are found to be very similar, one expects to see much bigger differences in the cross sections when starting from excited states. For example, in the case of the ^{1,3}P states, the two valence electrons in Be have the same principal quantum number, a similar radial extent, and are thus more strongly correlated than the $1s$ and $2p$ electrons in the ^{1,3}P states of helium. Moreover, as shown in a recent experiment [25] on atomic lithium, the particular symmetry of the target initial state can profoundly impact the consequences of double photoionization. These considerations offer new opportunities to study DPI from non-spherical atomic targets with the robust methods presented here. Work on DPI from excited Be is underway and will be report in a future publication.

ACKNOWLEDGMENTS

This work was performed under the auspices of the US Department of Energy by the Los Alamos National Laboratory and the University of California Lawrence Berkeley National Laboratory under Contract DE-AC02-05CH11231 and was supported by the US DOE Office of Basic Energy Sciences, Division of Chemical Sciences. CWM acknowledges support from the National Science Foundation (Grant No. PHY-0604628).

[1] T. N. Rescigno and C. W. McCurdy, Phys. Rev. A **62**, 032706 (2000).
[2] C. W. McCurdy, M. Baertschy, and T. N. Rescigno, J. Phys. B **37**, R137 (2004).
[3] F. L. Yip, D. A. Horner, C. W. McCurdy, and T. N. Rescigno, Phys. Rev. A **75**, 042715 (2007).
[4] W. Vanroose, D. A. Horner, F. Martín, T. N. Rescigno, and C. W. McCurdy, Phys. Rev. A **74**, 052702 (2006).
[5] A. Palacios, T. N. Rescigno, and C. W. McCurdy, Phys. Rev. A **77**, 032716 (2008).
[6] A. Palacios, T. N. Rescigno, and C. W. McCurdy, Phys. Rev. A **79**, 033402 (2009).
[7] J. Feist, S. Nagele, R. Pazourek, E. Persson, B. I. Schneider, L. A. Collins, and J. Burgdörfer, Phys. Rev. A **77**, 043420 (2008).
[8] S. Fraga, J. Karkowski, and K. M. S. Saxena, in *Handbook of Atomic Data* (Elsevier, Amsterdam, 1976).
[9] A. S. Kheifets and I. Bray, Phys. Rev. A **65**, 012710 (2001).
[10] J. Colgan and M. S. Pindzola, Phys. Rev. A **65**, 022709 (2002).
[11] F. Citrini, L. Malegat, P. Selles, and A. K. Kazansky, Phys. Rev. A **67**, 042709 (2003).
[12] S. Laulan and H. Bachau, Phys. Rev. A **69**, 033408 (2004).
[13] D. C. Griffin, M. S. Pindzola, C. P. Ballance, and J. Colgan, Phys. Rev. A **79**, 023413 (2009).
[14] R. Wehlitz and S. B. Whitfield, J. Phys. B **34**, L719 (2001).
[15] D. Lukic, J. B. Bluett, and R. Wehlitz, Phys. Rev. Lett. **93**, 023003 (2004).
[16] R. Wehlitz, D. Lukic, and J. B. Bluett, Phys. Rev. A **71**, 012707 (2005).
[17] D. A. Horner, J. Colgan, F. Martín, C. W. McCurdy, M. S. Pindzola, and T. N. Rescigno, Phys. Rev. A **70**, 064701 (2004).
[18] E. Lindroth, H. Persson, S. Salomonson, and A.-M. Mårtensson-Pendrill, Phys. Rev. A **45**, 1493 (1992).
[19] M. O. Krause and C. D. Caldwell, Phys. Rev. Lett. **59**, 2736 (1987).
[20] P. Selles, L. Malegat, and A. K. Kazansky, Phys. Rev. A **65**, 032711 (2002).
[21] F. Maulbetsch and J. S. Briggs, J. Phys. B **28**, 551 (1995).
[22] A. Huetz, P. Selles, and D. W. J. Mazeau, J. Phys. B **24**, 1917 (1991).
[23] A. S. Kheifets and I. Bray, Phys. Rev. A **73**, 020708(R) (2006).
[24] F. Maulbetsch and J. S. Briggs, J. Phys. B **26**, 1679 (1993).
[25] G. Zhu, M. Schuricke, J. Steinmann, J. Albrecht, J. Ullrich, I. Ben Itzhak, T. J. M. Zouros, J. Colgan, M. S. Pindzola, and A. Dorn, Phys. Rev. Lett. **103**, 103008 (2009).